LANGMUIR

pubs.acs.org/Langmuir Article

Dielectric-Loaded Waveguides as Advanced Platforms for Diagnostics and Application of Transparent Thin Films

Quaid Zaman,* Jefferson S. Costa, Tahir, Arthur R. J. Barreto, Jefferson F. D. F. Araujo, Luís D. Carlos, Albano N. Carneiro Neto, Marco Cremona, Zubair Ahmed, André Felipe S. Cruz, Nadson Welkson P. Souza, Karlo Q. da Costa, Victor Dmitriev, Anna Laurenzana, Francesca Margheri, and Tommaso Del Rosso*

Cite This: *Langmuir* 2021, 37, 3248−3260 Read Online

ACCESS | Metrics & More | Article Recommendations | Supporting Information

ABSTRACT: An alternative approach to classical surface plasmon resonance spectroscopy is dielectric-loaded waveguide (DLWG) spectroscopy, widely used in the past decades to investigate bio-interaction kinetics. Despite their wide application, a successful and clear approach to use the DLWGs for the one-step simultaneous determination of both the thickness and refractive index of organic thin films is absent in the literature. We propose here, for the first time, an experimental protocol based on the multimodal nature of DLWGs to be followed in order to evaluate the optical constants and thickness of transparent thin films with a unique measurement. The proposed method is general and can be applied to every class of transparent organic materials, with a resolution and accuracy which depend on the nature of the external medium (gaseous or liquid), the geometrical characteristics of the DLWG, and the values of both the thickness and dielectric constant of the thin film. From the experimental point of view, the method is demonstrated in a nitrogen environment with an accuracy of about 3%, for the special case of electroluminescent thin films of Eu^{3+} β-diketonate complexes, with an average thickness of about 20 nm. The high value of the refractive index measured for the thin film with the $Eu(btfa)_3(t\text{-}bpete)$ complex was confirmed by the use of a spectroscopic model based on the Judd−Ofelt theory, in which the magnetic dipole transition $^5D_0 \rightarrow {}^7F_1$ (Eu^{3+}) for similar films containing Eu^{3+} complexes is taken as a reference. The DLWGs are finally applied to control the refractive index changes of the organic thin films under UVA irradiation, with potential applications in dosimetry and monitoring light-induced transformation in organic thin films.

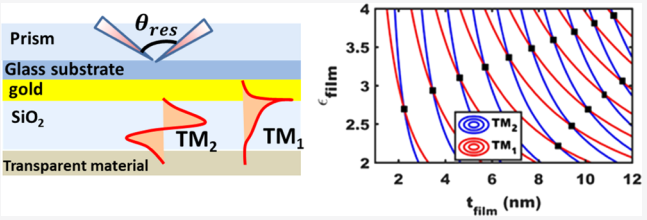

1. INTRODUCTION

The principal optical techniques used for transparent thin-films characterization are ellipsometry[1−4] and surface plasmon resonance spectroscopy (SPR).[5,6] Classical ellipsometry techniques give accurate results in a broad range of wavelengths, but the analysis of the experimental data used to calculate the parameters of interest of the thin films (dielectric constant, ε_{film}; thickness, t_{film}) is performed using complicated theoretical models.[7,8] In this scenario, SPR-based characterization represents an alternative approach. SPR spectroscopy based on Kretschmann configuration is in fact a well-established optical technique in which the surface plasmons are excited by an incoming TM-polarized light coupled to the conduction electrons of a thin metal film.[9] Since the evanescent field of the surface plasmon is highly sensitive to the small refractive index changes at the metal−dielectric interface, it can be effectively employed not only for the real-time monitoring of (bio)chemical interactions[10,11] but also for the characterization of organic ultrathin films.[5,6,12]

Similar to classical ellipsometry, in SPR spectroscopy, the main challenge is the simultaneous determination of optical constants and thickness of organic thin films. For example, in the case of SPR spectroscopy performed at a unique wavelength, the direct inversion of phase and intensity of reflected waves into the thickness and refractive index of the thin film under investigation is not possible, since all the parameters are inseparable in Fresnel's multilayer reflectance equations. Therefore, the prior knowledge of either the thickness or dielectric constant of the organic thin film is necessary and has to be accomplished by alternative techniques. This is a well-known problem in the field, and various groups have attempted to overcome it by considering at least two independent set of measurements for the same sample, varying experimental parameters such as the wavelength of the electromagnetic (EM) radiation,[13] the thickness

Received: September 29, 2020
Revised: February 22, 2021
Published: March 8, 2021

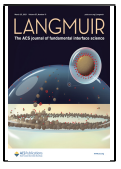

https://dx.doi.org/10.1021/acs.langmuir.0c02862
Langmuir 2021, 37, 3248−3260

of the thin films,[8] or the refractive index of the external medium.[7,14]

The latter method, where the SPR spectra are measured in two different external environments, is applicable only for the characterization of ultrathin film ($t_{film} \approx 1$ nm) of transparent materials; however, the interaction with different external fluids might induce different organization of organic molecules. In the two-wavelength approach,[13] the knowledge of the dispersion function of the transparent layer is needed, which may not be possible when considering the synthesis of new functional materials. A two-film thickness (TFT) technique[8] has been recently applied by our group for the full characterization of luminescent organic materials but is limited by the assumption of the prior knowledge of the ratio of the nominal thickness of the two thin films.

In the present research, we will demonstrate that the use of multimodal dielectric-loaded waveguides (DLWGs)[9,14,15] offers a convenient way to overcome the problems reported above and provides an elegant tool to assess simultaneously the determination of both the thickness and refractive index of the transparent thin films by one unique measurement.

In the literature, Salamon et al.[15] and Knoll[16] independently proposed for the first time the use of SPR-based DLWG spectroscopy for the characterization of bio-interfaces, thin-organic films, and the monitoring of bio-interaction kinetics. Recently, DLWG spectroscopy has been applied in metal-nanoparticle counting[17] or to monitor the changes in thickness and refractive index of plasma-polymerized allylamine thin films in humid and aqueous media.[18] Similarly, Akhavan et al. studied the inhomogeneity of the plasma-polymerized acrylic acid (PPAc) thick film from the combination of SPR and waveguide (WG) modes.[19] In the latter case, quantitative evaluation of the reflectivity spectra was carried out by varying the refractive index and thickness of the PPAc film to achieve the best theoretical fit on the experimental data. However, the experimental approach presented in all these experiments[15−19] needs previous knowledge of the dielectric constant or thickness of the thin film, in order to obtain the fit of the measured SPR/WG reflectivity spectra, thus limiting the use of these methods for the characterization of organic thin films based on new materials. In the present research, we propose for the first time, what might be called a dual-modal method, which uses the multimodal character of the WGs for the simultaneous evaluation of the values of both t_{film} and ε_{film} of the transparent thin film under investigation.

A second point that is underestimated in many cited experimental works is the accurate determination of the optical constants and thickness of the bilayer (Au SiO_2), which critically affects the accuracy of the DLWG in thin-film characterization.

Hence, the experimental part of this work dedicated to SPR measurements, starts with the description of a protocol that researchers have to apply to establish the accuracy of their DLWG sensing platforms in the experimental determination of both t_{film} and ε_{film}. From the theoretical point of view, we show how the resolution and accuracy of the DLWGs strongly depend on the geometrical characteristics of the WG, the thickness, and the dielectric constant of the transparent thin film to be characterized, as well as the environment in which the spectroscopy is performed. From an experimental point of view, the method is demonstrated for the special case of luminescent thin films of Alq_3, $Eu(dbm)_3$phen, and $Eu(btfa)_3$(t-bpete) in a nitrogen-controlled environment, with an average thickness of about 20 nm and a refractive index ranging approximately from 1.5 to 1.9.

The thickness range (tens of nm) investigated in this research is particularly interesting for two reasons: (i) it is too high to apply the two-wavelength[7] or two-medium[13] methods proposed in the literature for ultra-thin films, and (ii) it is the typical thickness of luminescence-active or charge-transporting layers in organic electronics.[20,21] Concerning the choice of the materials, luminescent lanthanide complexes with attached organic ligands have been largely investigated in the literature because of their unique spectral properties of intra 4f−4f emission, such as the characteristic narrow emission bands and a long emission lifetime over a wide range of wavelengths (ultraviolet/visible/near-infrared). These characteristics enable them to have a wide application in displays, lighting, organic light-emitting diode devices, sensors, and solar cells.[20,22] Despite the advances in luminescent lanthanide complex-based devices, the knowledge of the optical properties and the relative environmental stability of these materials is still limited. In this sense, we recently observed a strict correlation between the quenching of photoluminescence (PL) and refractive index increase for thin films of $Eu(dbm)_3$phen under controlled UVA (360 nm) radiation.[23] The experimental results of the present research confirm that general metal/β-diketonate complexes are optimal candidates for the development of compact UVA optical dosimeters.[23] The high experimental value of the refractive index measured for the $Eu(btfa)_3$(t-bpete) thin film is supported by the introduction of a spectroscopic model based on Judd−Ofelt theory, where the $^5D_0 \rightarrow {}^7F_1$ emission has a key role.

Although the DLWG-based monitoring of both t_{film} and ε_{film} under EM external irradiation has been demonstrated for the special case of luminescent Eu^{3+} β-diketonate complexes, the presented technique can be useful for transparent materials of different nature, independent of the deposition technique (evaporation,[8] ligand fluxing,[10] magnetic,[24] etc.), with important applications in the fields related to light-induced physical−chemical transformations, including polymerization[18,25] or photomechanical effect,[26] among the most.

2. MATERIALS AND METHODS

2.1. Materials. Gold pellets purchased from the Kurt J. Lesker Company with purity better than 99% were used for the deposition of plasmonic thin films. Ethanol, acetone, 3-mercaptopropyltrimethoxysilane (MPTS), and trichloroethylene purchased from Sigma-Aldrich were used without further purification. The ultrapure Milli-Q water was taken from a purification system (Millipore, USA). $Eu(dbm)_3$(phen) and Alq_3 powders were purchased from Lumtec (Taiwan) with purities better than 99.5 and 99%, respectively. $Eu(btfa)_3$(t-bpete) synthesized from our collaborator was used as received.[27] As an epoxy-based adhesive, we purchased the commercial epoxy Araldite (two components, 10 min cure).

2.2. UV Irradiation and PL Spectroscopy. The PL spectra of the thin films of Eu β-diketonate complexes were measured using a Photon Technology International (PTI) fluorescence spectrometer, model QuantaMaster 40. The PL spectra, excited at $\lambda = 360$ nm, were taken at steps of 1 nm, with a wavelength resolution better than 1 nm and an integration time of 0.2 s. For the degradation experiments, the metal−organic devices were irradiated in situ using a UV lamp, followed by a band-pass optical filter with 70% transmission in the spectral window between 300 and 400 nm. The optical irradiance reaching the sample was adjusted using neutral filters. The UV irradiance was measured using a UV-enhanced silicon photodetector from Newport (U.S.A., model 818-UV/DB UV).

https://dx.doi.org/10.1021/acs.langmuir.0c02862
Langmuir 2021, 37, 3248−3260

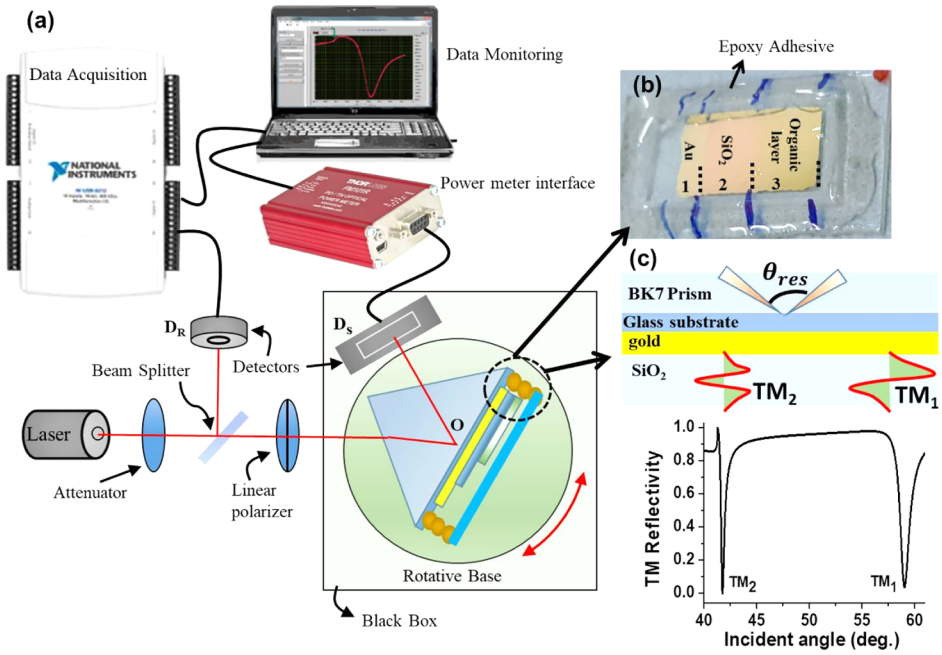

Figure 1. (a) Schematic representation of the experimental setup used for DLWG thin-film characterization. (b) Photo of one of the fabricated samples, indicating the regions with different thin films: Au monolayer (1), Au/SiO_2 bilayer (2), and organic material over DLWG (3). The samples were sealed in a nitrogen environment using an epoxy adhesive glue. (c) Scheme illustrating the individual layers of the DLWGs, the theoretical E-near-fields, and the SPR reflectivity curves.

2.3. Fabrication of DLWG Platforms and Samples with Organic Thin Films. The detailed fabrication procedure of the DLWGs is reported elsewhere.[14] Briefly, an Au thin film of about 47 nm is initially deposited on pre-cleaned BK7 glass substrates, properly functionalized with a self-assembled monolayer (SAM) of 3-mercaptopropyltrimethoxysilane (MPTS).[28] The Au-coated glass is inserted into deionized water for 24 h to stabilize the metal−glass interface, as suggested by different authors.[29,30] The fabrication of the DLWGs is completed by the hydrolysis and condensation of a SAM of MPTS on the thin gold surface[14] and the subsequent deposition of a ∼600 nm thick dielectric layer of SiO_2.

Finally, the thermal depositions of Alq_3, $Eu(dbm)_3Phen$, and $Eu(btfa)_3(t\text{-}bpete)$ thin films were performed on Au/SiO_2 bilayers at a rate of 1 Å/s with a pressure of 1.8×10^{-6} mbar, using a Leybold Univex 300 thermal deposition system, integrated into a customized MBraun glovebox with a gas purification system. The layer thickness was controlled in situ through a quartz crystal monitor and confirmed by profilometry measurements. The multilayered structure was kept in a nitrogen environment and eventually encapsulated by bonding a clean quartz slide on the upper side of the sample with a thin bead of an epoxy-based adhesive in a similar way as reported in ref 8.

2.4. Experimental Protocol for the Characterization of the Au/SiO_2 Bilayers. The SPR spectrometer in the Kretschmann configuration used for the experimental measurements is shown in Figure 1. The setup is identical to the one described in detail in ref 17, where a black box is used to keep the sample under dark conditions. The laser beam comes from a linearly polarized source at the wavelength of 633 nm (Thorlabs U.S.A., model HNL050LB, He−Ne, 5 mW) or 783 nm (Ondax U.S.A., model LM-783-PLR-75-1, 75 mW). The beam splitter deflects the incident beam to a photodetector D_R (Thorlabs U.S.A., model DET36A/M, Si detector, 350−1100 nm, 14 ns rise time, 13 mm^2), which measures the input intensity of the beam. The signal detector D_s inside the black box is a photodiode sensor (Thorlabs U.S.A., model S170C, 350−1100 nm, 100 mW), with a large 18 × 18 mm^2 sensor-active area. The photodetectors D_R and D_S are interfaced to a personal computer by a data acquisition board (National Instruments, U.S.A., model USB-6501, 24 channels) and a power-meter interface enabling both the USB and RS232 operation (Thorlabs U.S.A., model PM101R), respectively. The rotation base of Sigma-Koki (model SGSP-80, Japan) has an angular resolution of 0.0025°.

The thickness and complex dielectric constant of the metal layer supporting the plasma wave were retrieved using Winspall 3.02[31] free software, while the codes used for the determination of the parameters of SiO_2 and organic thin films, and the accuracy of the obtained values, were developed using MatLab 9.0 software, applying the transfer-matrix method.[32]

To assess the potentialities of our fabricated DLWGs for the accurate determination of ε_{film} and t_{film}, it is necessary to first characterize the Au/SiO_2 bilayers. To perform this task, the deposition of different materials was not done on the whole surface of the sample. Figure 1b presents the three different regions of interest of the sample. The regions are well separated to be characterized independently, in the following order: the Au monolayer (region 1), the Au/SiO_2 bilayer (region 2), and the whole organic thin film supported on the DLWG (region 3). The optical constants and thickness of the Au monolayer measured in region 1 are used as input information to retrieve the parameters of the SiO_2 thin film in the measurement of region 2. The same concept is repeated for the final characterization of the organic thin films, where the experimental parameters of SiO_2 obtained in step 2 are used as input data. This procedure is used both to determine and limit the uncertainty in the final measurements of the optical constants of the organic thin films. In fact, without a previous accurate experimental measurement of the optical parameters of the DLWGs, a low accuracy in the determination of ε_{film} and t_{film} is expected due to the arbitrary choice of the values which can be used to fit the Au/SiO_2 bilayer reflectivity spectra. Figure 1c schematically shows each layer of the DLWGs and the reflectivity dips associated with the excitation of TM_1 and TM_2 WG modes in a nitrogen (air) environment, at the wavelength of 633 nm. The simulations were performed considering the experimental thickness and dielectric constant of the individual Au and SiO_2 layers.

Due to the degradation processes observed for BK7/Au and Au/SiO_2 interfaces in contact with air,[28] the quality of the encapsulation process has to be tested before starting any optical characterization of the multilayer structure. This is done by the real-time monitoring of the resonance angles θ_{TM2} and θ_{TM1} over a time of about 24 h.

https://dx.doi.org/10.1021/acs.langmuir.0c02862
Langmuir 2021, 37, 3248−3260

To conclude, four important experimental factors have to be considered for experimental groups aiming to use DLWGs for the characterization of transparent thin films using the proposed configuration:

(a) the laser incidence point O on the BK7 prism (Figure 1a) must coincide with the central axes of the supporting rotation base. If this task is not accomplished, the point O will move on the surface of the sample during the base rotation scanning different regions;
(b) the signal detector D_s in the black box needs to have a large active window because the SPR spectra of the organic thin film over the DLWGs extend along a wide angular range;
(c) the SPR reflectivity curve of the organic thin film over the DLWGs has to be recorded only after the characterization of the thickness and dielectric constant of both the Au and SiO_2 thin films;
(d) the control of the stability of the angles of the multiple resonances of the DLWGs is necessary prior to the final characterization of the transparent thin film.

2.5. Fitting Procedure Used for the Determination of the Thickness and Refractive Index of the Layers. As shown in the theoretical SPR spectra reported in Figure 1c, the fabricated DLWGs are characterized by two reflectivity dips in TM polarization and nitrogen (or air) environment. The high angular one corresponds to the TM_1 mode, while the thinner resonance at lower incidence angles corresponds to the TM_2 mode. It is the presence of multiple WG resonance modes which allow the single-measurement determination of both the thickness and dielectric constant of the SiO_2 as well as the organic thin film.

In the proposed two-modes method, the theoretical fit of the experimental results is not performed simultaneously on both the modes (TM_1 and TM_2 in our case). First, we scan the possible (ε_{film}, t_{film}) couples which allow the matching between the theoretical and experimental angular values of the TM_1 resonance. In the second step, the same procedure is applied for the TM_2 mode. In this way, we obtain two set of solutions $(t, \varepsilon)_{TM1}$ and $(t, \varepsilon)_{TM2}$ for the dielectric constant and the thickness of the thin film under investigation, each one associated with a different mode. As reported for the two-color method,[13] the intersection point of the two curves in the ε versus t plane represents the real value of the parameters. This fitting procedure has been used for both SiO_2 and organic thin films characterization. To perform the fitting, we developed a code using MatLab 9.0 software based on the classical transfer matrix method,[32] which calculates the reflectivity curves of planar multi-layer systems. For the final characterization of the organic thin film, we fix the values of the parameters of the Au/SiO_2 bilayer measured experimentally and vary the values of ε_{film} and t_{film} of the organic layer to match the experimental angle of resonance shifts for both the modes.

3. RESULTS AND DISCUSSION

3.1. Characterization of the SiO_2 Layer Using the two-modes method. As introduced in Section 2.4, the DLWGs have to be accurately characterized before the investigation of the transparent thin films. In Table 1 are reported the values of the thickness and complex dielectric function of the metal and dielectric layers, at the wavelength of 633 nm.

Region 1 of the sample, consisting of the Au bare thin film, is the first one to be characterized by SPR spectroscopy. The values of t_{Au} and ε_{Au} are obtained using the free Winspall 3.02[31] software, easily achievable by all the laboratories dedicated to SPR spectroscopy.

Angular scanning of the reflectivity of the Au/SiO_2 bilayers (region 2) leads to the experimental determination of the resonance angles $\theta_{TM2} = 41.745°$ and $\theta_{TM1} = 59.030°$, as represented in Figure 2a. With the particular thickness of the SiO_2 layer of the fabricated DLWGs, it is not possible to excite the TM_0 mode, at least when nitrogen (air) is used as the external medium. In the two-modes analysis method, the experimental angles of resonance are separately fitted to obtain two infinite set of couple of values $(t_{SiO_2}, \varepsilon_{SiO_2})_{TM1}$ and $(t_{SiO_2}, \varepsilon_{SiO_2})_{TM2}$, making use of the optical parameter values of the Au thin film listed in Table 1. These two set of values are represented in Figure 2b in the $(t_{SiO_2}, \varepsilon_{SiO_2})$ plane, yielding an intersection point at 591.7 nm and 2.052, which represents the actual values of the thickness and dielectric constant of the silica layer, respectively.

Table 1. Thickness and Dielectric Constant of Au and SiO_2 Thin Films at the Wavelength of 633 nm[a]

layer	t (nm)	ε_r	ε_i	$\delta\varepsilon_r$ (%)	$\delta\varepsilon_i$ (%)	δt (%)
Au	46.8	−11.54	1.47	0.5	5	1
SiO_2	591.7	2.052	0	0.04		0.08

[a] $\delta\varepsilon_r$, $\delta\varepsilon_i$, and δt, represent the experimental accuracies in the determination of the real and imaginary parts of the dielectric constant and the thickness of the thin films.

The stability of the DLWG encapsulated in the nitrogen environment was monitored for 24 h before starting the experimental characterization of the thin films, as represented in Figure 2c, where the experimental reflectivity curve was taken at the wavelength of 783 nm. Figure 2d highlights the change in time of the resonance angles θ_{TM2} and θ_{TM1}, where the maximum observed shift is of the order of the accuracy in the experimental determination of zero angle, which is of the order of ± 0.01°. The results demonstrate the stability of the encapsulated DLWG structure, which is the first step to be assessed in accurate SPR-based thin-film characterization.

In a previous work,[8] we evaluated the experimental accuracies $\delta\varepsilon_r$, $\delta\varepsilon_i$, and δt in the determination of the real and imaginary parts of the dielectric constant and in the thickness of the Au thin film. These accuracies, listed in Table 1, represent a source of experimental error in the determination of the optical constants and thicknesses of the SiO_2 and the transparent thin film. Indeed, the uncertainties propagate and influence the determination of the crossing point of the curves representing the possible values in the plane t_{SiO_2} vs ε_{SiO_2} (Figure 2b). The values of t_{Au} and ε_{Au} are therefore varied in a range coherent with the experimental accuracies reported in Table 1, and the possible crossing points are calculated. The systematic error in the experimental determination of the zero angle (±0.01°) is finally taken into account by repeating the procedure described above but shifting both the experimental angles of resonances $\theta_{TM2} = 41.745°$ and $\theta_{TM1} = 59.030°$ in the positive (+0.01°) or negative (−0.01°) direction. This process leads to the final accuracies $\delta\varepsilon_{r\,SiO_2}$ and δt_{SiO_2} reported in Table 1.

3.2. Two-Mode Method for the Characterization of Alq_3 and Eu β-Diketonate Complex Thin Films. Thin films of Alq_3, $Eu(dbm)_3phen$, and $Eu(btfa)_3(t\text{-}bpete)$ were deposited over the DLWGs with a nominal thickness (as read by the crystal balance in the thermal deposition apparatus) of 25, 27, and 20 nm, respectively. The final samples had the appearance shown in Figure 1b. The DLWG diagnostic platforms were characterized as described above, and a last reflectivity angular scanning was performed over the whole three-layered structures in their corresponding region 3.

https://dx.doi.org/10.1021/acs.langmuir.0c02862
Langmuir 2021, 37, 3248−3260

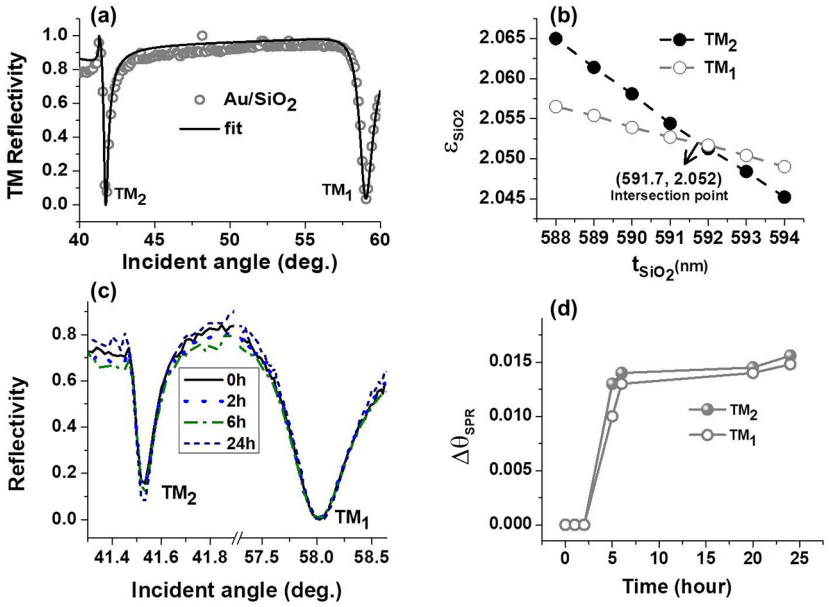

Figure 2. (a) Angular reflectivity spectra of the encapsulated DLWGs showing the excitation of TM_1 and TM_2 modes at the wavelength of 633 nm. The experimental points (open circles) were fitted using the MatLab home-made code (solid line). (b) Illustration of the two-modes approach for the one-step determination of both the thickness and dielectric constant of the SiO_2 thin film. The two set of values $(t_{SiO_2}, \varepsilon_{SiO_2})_{TM1}$ and $(t_{SiO_2}, \varepsilon_{SiO_2})_{TM2}$ yield an intersection point at 591.7 nm and 2.052. (c) Time dependence of the angular reflectivity curves of the encapsulated DLWGs in the nitrogen environment over 24 h. The wavelength of the laser beam was 783 nm. (d) Time-dependence of the resonance angles θ_{TM2} and θ_{TM1} of the reflectivity spectra shown in part (c) over 24 h.

As represented in Figure 3, in all samples, the TM_1 mode was observed at incidence angles higher than 60°, so that it is fundamental to use a signal detector with a large active window, as highlighted in Section 2.4. In Figure 3a,c,e, together with the experimental results are also reported the corresponding theoretical fit, as continuous curves. The latter ones are obtained by considering for the Au/SiO_2 bilayer the results listed in Table 1, and for the values of thickness and dielectric constant of the organic thin film, the results obtained by the application of the two-mode method are considered, similarly as performed for the SiO_2 layer. The curves in the ε versus t plane and the corresponding intersection point for all the organic materials under observation are reported in Figure 3b,d,f.

In the case of Alq_3 thin films, we obtained t_{Alq_3} = 25.6 nm and ϵ_{Alq_3} = 3.05, corresponding to the refractive index n_{Alq_3} = 1.75. The validation of the method was performed comparing this value with the one obtained using the TFT method on monomodal SPR platforms, which we demonstrated successfully in previous work.[8] As shown in the Supporting Information section, using the TFT method, we obtained a value of 1.74, which validates the proposed multimodal approach. The results are also consistent with the value obtained in the literature by the use of other optical techniques, as reported in Table S1.

For the $Eu(dbm)_3phen$ thin film, we obtained a value of the refractive index of 1.55 at 633 nm, which is coherent with the results reported in the literature.[33,34] In the latter case, the calculation of the experimental Judd−Ofelt intensity parameters for the Eu^{3+} ion in the complexes requires the knowledge of the average refractive index of the material. These parameters were determined from the emission intensities of the $^5D_0$ to ^7F_J (J = 2, 4) electronic transitions of Eu^{3+} by assuming some reasonable value for the refractive index (1.5).[35] Our experimental result showed an excellent match with the assumed value of the refractive index in the calculation of the parameters for the Eu^{3+} ion. Also, this agreement supports the validity of the multimodal analysis.

3.3. Limits in the Performance of the Proposed DLWGs as Thin-Film Characterization Platforms: Sensitivity, Resolution, Accuracy, and Range. In the present section, we describe in detail the sensitivity, resolution, and accuracy of the proposed DLWG platforms in the measurement of both the thickness (t_{film}) and dielectric constant (ε_{film}) of the thin film. Our calculations are based on the following input experimental values: (1) resolution in the angular shift of the SPR spectrometer, (2) uncertainty in the zero-angle determination, and (3) accuracy in the determination of the parameters of the gold thin film deposited on the glass BK7 slide (Table 1).

3.4. Sensitivity and Resolution. Although the angular resolution of the mechanical base (Sigma-Koki, model SGSP-80, Japan) used to scan the reflectivity curve is 0.0025°, standard SPR spectrometers based on angular interrogation can resolve the shift of the SPR curve with a typical angular resolution of about 10^{-4} degrees.[36,37] The experimental setup used in the present research is not new and has been tested in different sensing applications[14,17,23] in which we could easily resolve an angular shift of the SPR curves of about 0.005°. Although the last value does not represent the best resolution of our experimental SPR setup, we will consider it as a conservative estimate of the angular-shift resolution, which will be used for the evaluation of the minimal thickness of the thin film which can be experimentally resolved.

In Figure 4a, we show the sensitivity (S) of the TM_2 (blue lines) and TM_1 (red lines) modes of the DLWG in an air environment. In Figure 4b, S is instead represented for the TM_1 (red lines) and TM_0 (green line) modes of the DLWG,

https://dx.doi.org/10.1021/acs.langmuir.0c02862
Langmuir 2021, 37, 3248−3260

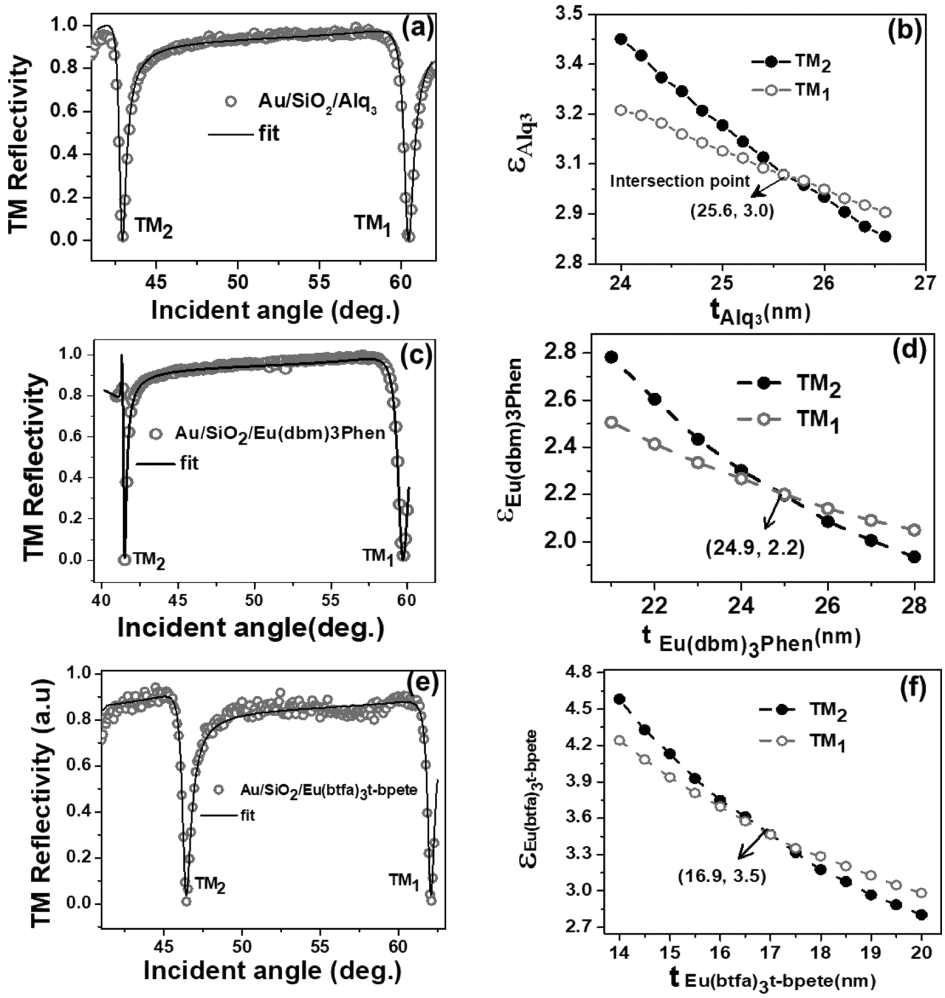

Figure 3. Left: Experimental reflectivity spectra obtained using TM polarized light (open circles) at the wavelength of 633 nm and the corresponding theoretical fits (solid lines). Thin films of (a) Alq_3, (c) $Eu(dbm)_3phen$, and (e) $Eu(btfa)_3(t\text{-}bpete)$ were analyzed. The trial curves corresponding to TM_1 (open circles) and TM_2 (filled circles) modes represent all the possible combination of thicknesses and dielectric constants of the organic thin films which fit the experimental reflectivity curve: (b) Alq_3, (d) $Eu(dbm)_3phen$, and (f) $Eu(btfa)_3(t\text{-}bpete)$. The intersection point corresponds to the actual values for the parameters of the organic thin film.

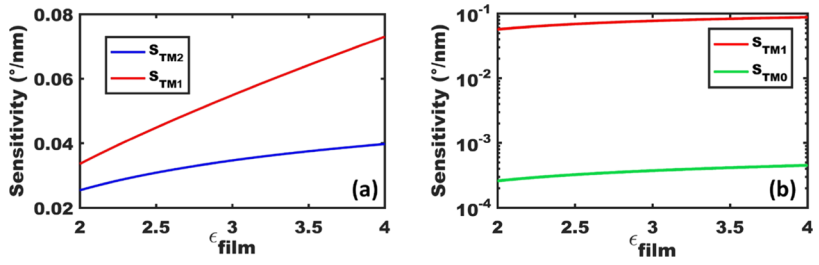

Figure 4. Sensitivity (S) of the TM_2 (blue line), TM_1 (red lines), and TM_0 (green line) modes of the DLWGs expressed as the angular variation of the SPR angle ($\Delta\theta_{spr}$) per unit of thin-film thickness (°/nm). (a) Air as the external medium. (b) Water as the external medium. The values of the parameters of the Au/SiO_2 bilayer are reported in Table 1. The excitation wavelength is 633 nm.

when water is used as the external medium. In both cases, S is expressed as the angular variation of the SPR angle ($\Delta\theta_{SPR}$) per unit thin-film thickness (°/nm). We highlight here that the thickness of the SiO_2 layer of the WGs fabricated in the present research does not allow the propagation of TM_2 modes at the wavelength of 633 nm when water is considered as an external environment. To evaluate the resolution of the DLWGs in thin-film characterization for values of ε_{film} between 2 and 4, we calculated the minimal thickness t_{film} of the transparent thin film deposited over the Au/SiO_2 bilayer, for which the angular displacements of the TM_0 ($\Delta\theta_{TM0}$), TM_1 ($\Delta\theta_{TM1}$) and TM_2 ($\Delta\theta_{TM2}$) modes are higher than 0.005°. The results are shown in Figure 5, considering both air (left panel) and water (right panel) as external media. Herein, the white region in the graphs corresponds to the couple of values in the (ε_{film}, t_{film}) plane for which $(\Delta\theta_{TM0}, \Delta\theta_{TM1})_{water}$ and $(\Delta\theta_{TM2}, \Delta\theta_{TM1})_{nitrogen/air}$ are higher than the angular displacement resolution.

https://dx.doi.org/10.1021/acs.langmuir.0c02862
Langmuir 2021, 37, 3248−3260

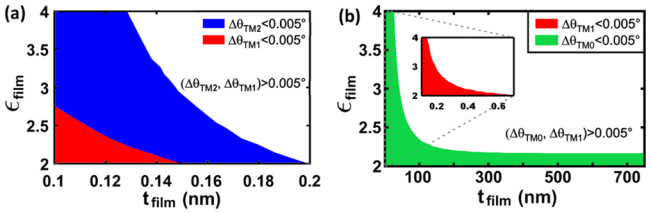

Figure 5. Thin-film thickness (t_{film}) and dielectric constant (ε_{film}) resolution of the DLWGs. (a) Air as the external medium. (b) Water as the external medium. In green, red, and blue colors are shown the regions of the values of ε_{film} and t_{film} for which the angular displacements of the TM_0 ($\Delta\theta_{TM0}$), TM_1 ($\Delta\theta_{TM1}$) and TM_2 ($\Delta\theta_{TM2}$) modes are, respectively, less than 0.005°. The values of the parameters of the Au/SiO_2 bilayer are reported in Table 1. The excitation wavelength is 633 nm.

Figure 6 represents the square of the component ($|H_y|^2$) of the magnetic field tangential to the interfaces of the multilayered structure constituting the DLWGs, in the case of both air (left panel) and water (right panel) as external media. The TM_0, TM_1, and TM_2 modes are associated with the green, red, and blue colors, respectively.

As visible in Figure 4, when air is used as an external environment, the sensitivity S of both TM_1 and TM_2 modes of the DLWGs lay in the range between 10^{-2} and 10^{-1} °/nm. Differently, when the water is the external medium, the sensitivity of the TM_0 mode is about $\sim 3 \times 10^{-4}$ °/nm, regardless of the value of ε_{film}. Coherent with these results, considerable differences are obtained in the study of the parameters of thin films (ε_{film}, t_{film}) whose adsorption onto the SiO_2 external surface can be angularly resolved by the DLWGs we have fabricated ($\Delta\theta_{SPR} > 0.005°$). The most critical situation is observed in water (Figure 5b), where the resolution of the DLWG might allow the detection of a deposition of transparent material only if the dielectric constant is higher than ~2.2, and if the thickness is higher than ~50 nm. When air is used as the external medium, a completely different behavior is observed. In this case, regardless of the value of the refractive index in the considered range ($2 < \varepsilon_{film} < 4$), the thickness resolution is of sub-nm (~0.2 nm).

The dependence of the resolution of the DLWG on different external environments can be understood by the analysis of the spatial distribution of the EM near-field associated with the WG modes in the different cases, as depicted for $|H_y|^2$ in Figure 6. In fact, an alternative way to investigate the sensitivity of SPR-sensing platforms is the evaluation of the field-matter integral,[38,39] which is a measure of the portion of the EM energy of the mode that is spatially overlapped with the thin film to be characterized. The EM evanescent fields of the TM_1 and TM_2 modes always present a portion of energy density at the interface between the SiO_2 layer and the external environment (where the transparent film is eventually deposited), whereas the energy density of the TM_0 mode is negligible at such interface when water is considered as the external medium. The same concept may be used to explain the increase in the sensitivity S of the modes for higher values of ε_{film}. For example, in Figure S2 is represented the $|H_y|^2$ profile associated with the TM_0 near-field when water is the external medium, depending on different values of ε_{film} and t_{film} = 100 nm. Thus, it is possible to see clearly that when the value of ε_{film} increases, a larger portion of the energy of the mode is confined in the region corresponding to the transparent thin film, leading to the increase of the sensitivity.

3.5. Accuracy. The accuracy of the DLWG-based ellipsometer was calculated considering as input data the accuracies reported in Table 1 for the characterization of the Au/SiO_2 bilayer. The parameters of the latter are hence varied in a range consistent with the value of Table 1, and the corresponding crossing points of Figure 3 are calculated again. This procedure is performed considering the experimental values of the angles of resonance of the TM_1 and TM_2 modes and repeatedly applying an angular shift of ±0.01° on the experimental reflectivity curves to take in account the contribution of the systematic error in the experimental determination of the zero angle. The accuracy in the determination of the dielectric constant ($\delta\varepsilon_{film\%}$) and the thickness ($\delta t_{film\%}$) of the transparent thin film is reported in Figure 7, where air was considered as the external medium, and

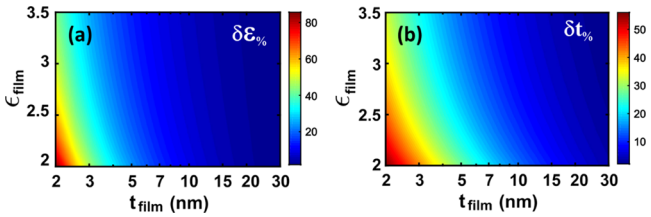

Figure 7. Mapping of the accuracy in the evaluation of the thickness (a) ($\delta\varepsilon_{film\%}$) and dielectric constant (b) ($\delta t_{film\%}$) of the transparent thin film in the (ε_{film} vs t_{film}) plane. Air is considered as the external medium. The values of the parameters of the Au/SiO_2 bilayer are reported in Table 1. The excitation wavelength is 633 nm.

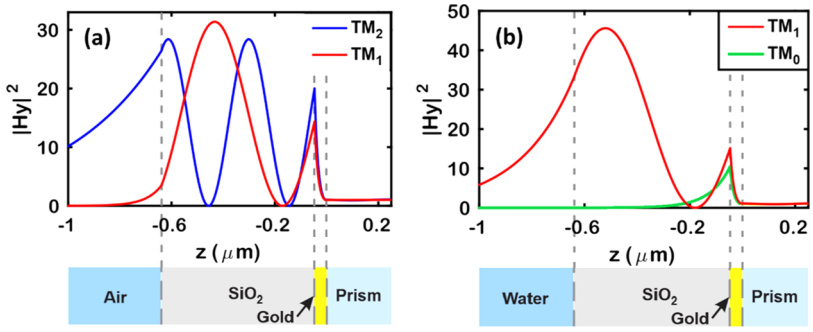

Figure 6. Square of the continuous magnetic near-field $|H_y|^2$ of (TM_1, TM_2) and (TM_0, TM_1) modes of the DLWGs in the absence of the transparent thin film in air (a) and water (b), respectively. At the bottom of the panels is represented the geometry of the multi-layered structure constituting the DLWGs. The values of the parameters of the Au/SiO_2 bilayer are reported in Table 1. The excitation wavelength is 633 nm.

https://dx.doi.org/10.1021/acs.langmuir.0c02862
Langmuir 2021, 37, 3248−3260

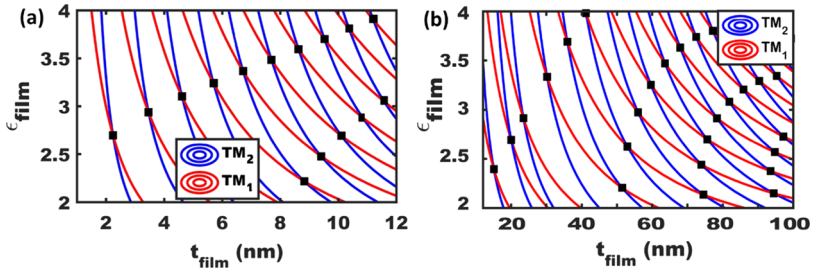

Figure 8. Crossing curves representing the possible couple of values (ε_{film}; t_{film}), associated with the TM_1 (red curve) and TM_2 (blue curves) modes for different transparent thin films deposited over the DLWGs. (a) $2 < \varepsilon_{film} < 4$; 1 nm < t_{film} < 12 nm. (b) $2 < \varepsilon_{film} < 4$; 12 nm < t_{film} < 100 nm. Air is considered as the external medium. The values of the parameters of the Au/SiO_2 bilayer are reported in Table 1. The excitation wavelength is 633 nm.

a color-based intensity scale is used. In Table S2 of the Supporting Information are listed the values of $\delta\varepsilon_{film\%}$ and $\delta t_{film\%}$ for some specific combinations of ε_{film} and t_{film}. The possible range of ε_{film} was considered between 2 and 3.5, while t_{film} was varied between 2.0 and 30.0 nm. A general trend is present, and we observe that the parameters of the thin film are evaluated with better accuracy by increasing both the thickness and the dielectric constant. Considering the lowest value of the refractive index ($n \approx 1.41$), thin films with thicknesses of 2.0, 5.0, 10, and 20 nm are characterized by values of the couple ($\delta\varepsilon_{film\%}$; $\delta t_{film\%}$) of about (56%; 86%), (29%; 25%), (14%; 10%), and (7%; 4%), respectively.

The particular trend in the accuracy is associated with the dependence on ε_{film} and t_{film} of the behavior of the crossing curves representing the possible couple of values (ε_{film}; t_{film}) associated with different modes of the DLWGs, as represented in Figure 8. We remember that each curve is associated with a particular angle of resonance of the TM_1 (θ_{TM1}—red curve) or TM_2 (θ_{TM2}—blue curve) modes. Hence, if we fix θ_{TM1}, by variation of θ_{TM2}, we will change the respective blue curve and we will have more intersection points with the same red line associated with θ_{TM1} as shown in Figure 8. In the case of panel (a), consecutive (red, blue) curves correspond to the angular variation of (θ_{TM1}, θ_{TM2}) of about (0.08°, 0.05°). The latter values are about (0.6°, 0.5°) in the case of panel (b).

Simulations were performed considering the values of the parameters of the Au/SiO_2 bilayer reported in Table 1 and transparent thin films with the dielectric constant between 2 and 4 and thickness between 1 and 12 nm [panel (a)], and between 12 and 100 nm [panel (b)]. In Figure 8, the black squares highlight the crossing points and correspond to the real value of ε_{film} and t_{film}. The trend of the slope of the crossing curves for different values of ε_{film} and t_{film} is particularly evident for thickness lower than 12 nm [panel (a)]. As both the thicknesses and dielectric constants of the thin film are decreased, the angle at the crossing points between the curves associated with the possible solutions for the TM_1 and TM_2 modes becomes smaller. Based on the procedure applied for the determination of the accuracy of the DLWG, the behavior of the crossing curves in Figure 8 clearly explains the results shown in Figure 7, where a worse accuracy is obtained for thin films with smaller values of ε_{film} and t_{film}.

3.6. Range. The dependence of the accuracy in the determination of ε_{film} and t_{film} for thin films with a dielectric constant of 2.0 and a thickness up to 250 nm in the air environment is represented in Figure S3. For both the thickness and dielectric constant, accuracy values lower than 1% are obtained when the thickness is higher than ~100 nm. When the thickness of an organic thin film with ε_{film} = 2.0 is increased beyond ~250 nm, a new TM_3 mode appears for the WG, as represented in Figure S4a. In such a case, θ_{TM1} reaches values of the order of ~65.0°. Higher angles start to be hard to be investigated experimentally, so that the monitoring of the angles of resonance of the TM_2 and TM_3 modes might be preferred up to a thickness of about 1.3 μm, for which also θ_{TM2} reaches values higher than 65.0°, and the observed modes should be changed again with the TM_3 and TM_4 modes, as shown in Figure S4b. Hence, using higher order couple of modes, our proposed approach may also be applied for the thicknesses of the thin film in the μm range. In Figure S4c,d, we show the accuracies $\delta\varepsilon_{film\%}$ and $\delta t_{film\%}$ for films with ε_{film} = 2.0 and thicknesses in the ranges (300−600 nm) and (1300−1500 nm), where (TM_2, TM_3) and (TM_3, TM_4) couple of modes have been used for the calculation. In both the cases, the calculated accuracy in the evaluation of ε_{film} and t_{film} is below 1%.

3.7. Improving the Performances of DLWG Thin-Film Characterization. It is important to highlight that the performance of the DLWGs as thin-film characterization platforms strictly depends on the geometrical parameters of the WG. As explained in Section 3.4 dedicated to sensitivity, the latter depends on the spatial overlap between the evanescent EM fields and the deposited thin film. Therefore, the SiO_2 layer thickness, the excitation wavelength, the metal substrate, and the order of modes may be properly chosen in order to maximize the field-matter integral, possibly leading to better sensitivity and accuracy. Although it is not the aim of the present research to find the experimental parameters to obtain the best resolution and accuracy, it is worth to put in evidence that the higher order modes should always be preferred to the TM_0 mode, which is characterized by the maximum intensity of the evanescent field at the Au/SiO_2 interface (Figure 6b) and is generally weak in the region beyond the SiO_2 layer, where the transparent thin film is deposited.

Our calculations show that the possibility to use higher order modes is particularly attractive to extend the application of the DLWGs in a water environment. As in the case of the transparent thin film under investigation, increasing the thickness of the SiO_2 layer leads to the appearance of modes with higher orders.[14,40] For example, Figure S5a shows the angular-dependent reflectivity spectra in the water environment (λ = 633 nm) of a DLWG with the same gold layer used in the present research (Table 1), and a SiO_2 film thickness of 1100 nm. Considering again a conservative angular resolution of 0.005° in the measurement of the angular shift of the resonances of the modes, monitoring the TM_1 and TM_2 modes

https://dx.doi.org/10.1021/acs.langmuir.0c02862
Langmuir 2021, 37, 3248−3260

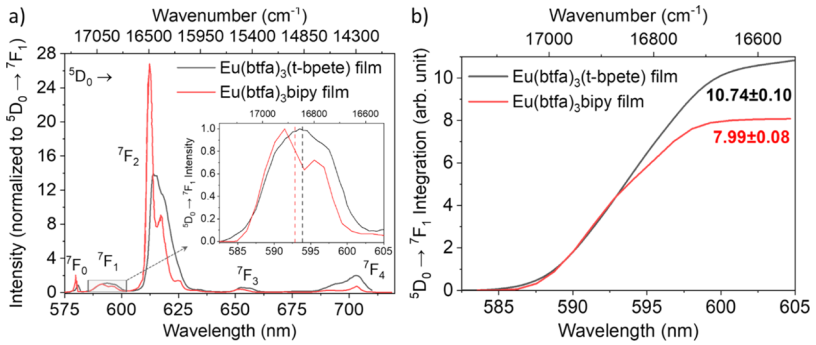

Figure 9. Comparisons between $Eu(btfa)_3bipy$ (red lines) and $Eu(btfa)_3(t\text{-}bpete)$ (black lines) thin films. Emission spectra for (a) $Eu(btfa)_3bipy$ (adapted from ref 49 with permission from Elsevier) and $Eu(btfa)_3(t\text{-}bpete)$ (this work) films, with excitation at 370 and 360 nm, respectively. The intensities were normalized according to the $^5D_0 \rightarrow {}^7F_1$ emissions, as visible in the inset. Their respective barycenters (592.8 and 593.9 nm or 16869 and 16838 cm^{-1}) are marked with dashed lines, as shown in the inset panel. (b) Integration ($S_{0\rightarrow1}$, from 582.5 to 605.0 nm) of the $^5D_0 \rightarrow {}^7F_1$ emission curve for each sample.

leads to a drastic change in the thin-film thickness resolution in a water environment, as shown in Figure S5b. In this case, on the basis of the approach described in Section 3.2, a thin film of tethered single-component ss-DNA (t_{film} = 6 nm; ε_{film} = 2.1)[41] might be, for example, characterized in terms of thickness and dielectric constant with an accuracy of the order of 8.4 and 1.7%, respectively.

Anyway, we highlight that the DLWG fabricated in the present research might also be used for the deposition of thin films formed in water by the use of flow cells,[14] and the thin films might be properly characterized after withdrawing the liquid in contact with the external surface of the sensing platform.

4. CONCLUSIONS ON THE PERFORMANCES OF THE DLWGS

To resume our results, when considering air as the external medium, the fabricated WGs have a resolution of about 0.2 nm for thin films with a dielectric constant of 2.0 (Figure 5a), but the accuracy in the determination of the parameters is higher than 100%. Concerning the range, if an accuracy better than ~15% is considered, the fabricated DLWGs can be successfully used for the characterization of transparent thin films with thickness between 5 nm and the μm range with values of the dielectric constant between 2 and 4.

We concluded that both DLWG thin-film characterization and classical ellipsometry may be performed in a range going from sub-nm to μm thick thin films.[42,43] Concerning the accuracy of classical ellipsometry, the definition of a general method for its determination is still a theme of debate,[44] although most of the companies producing the equipment claim an accuracy better than 1%[45] for sub-nm thick thin films also. In the case of DLWG spectroscopy, the accuracy strongly depends on the thickness and refractive index of the organic layer as well as on the geometrical characteristics of the WGs. Thus, in future studies, we aim to investigate the particular SiO_2 thickness, metal substrate, excitation wavelength, and particular couple of modes to be monitored to obtain the maximum field-matter integral, and hence the best accuracy and resolution, in both gaseous and liquid environments.

4.1. Spectroscopic Model Based on Eu^{3+} $^5D_0 \rightarrow {}^7F_1$ Intensity. In the case of organic luminescent thin films analyzed experimentally ($t_{film} \approx$ 20 nm), if small percentage differences are not considered, we can conclude that their dielectric constant and thickness were characterized by experimental accuracies of 4 and 3%, respectively (see Table S2). The special nature of the lanthanide β-diketonate complexes studied in the present research allows us to have an alternative control on our experimental results, which is particularly important to confirm the high value of the refractive index measured for the $Eu(btfa)_3(t\text{-}bpete)$ thin film.

In lanthanide spectroscopy, the electric dipole transitions between $^{2S+1}L_J$ and $^{2S'+1}L'_{J'}$ states ($|SLJ\rangle \rightarrow |S'L'J'\rangle$) have to obey the selection rule on the J quantum number, $|J - J'| \leq \lambda \leq J + J'$ (with λ = 2, 4, and 6), for nonzero $S'L'J'U^{(\lambda)}SLJ$ matrix elements.[46,47] In this sense, the Eu^{3+} ion has unique properties, especially regarding its emission spectrum where it is possible to directly obtain the Judd–Ofelt intensity parameters Ω_λ (λ = 2, 4, and 6) in terms of the integrated areas under the emission curves.[46] This is feasible due to the employment of the $^5D_0 \rightarrow {}^7F_1$ emission as an internal reference. This particular transition is forbidden by the electric dipole (from the above-mentioned selection rules), but it is allowed by the magnetic dipole one (whose selection rules are $|J - J'| = 0$ or 1, except for the case $J = J' = 0$).

The radiative rate $A_{0\rightarrow1}$ contribution of the $^5D_0 \rightarrow {}^7F_1$ transition (in units of s^{-1}) can be calculated as[46,48]

$$A_{0\rightarrow1}(n, \tilde{\nu}) = 0.31 \times 10^{-11} \cdot n^3 \cdot \tilde{\nu}^3 \quad (1)$$

where n is the refractive index which depends upon the wavelength λ and $\tilde{\nu}$ is the wavenumber corresponding to the barycenter of the $^5D_0 \rightarrow {}^7F_1$ transition.

Here, an alternative approach is proposed to predict the refractive index of $Eu(btfa)_3(t\text{-}bpete)$ using its $^5D_0 \rightarrow {}^7F_1$ emission. The $Eu(btfa)_3bipy$ film[49] was chosen as a reference, once the n (=1.61 ± 0.04) was also determined by ellipsometry at 632.8 nm, similarly to the case of the $Eu(btfa)_3(t\text{-}bpete)$ film. The structures of these Eu-based complexes are illustrated in Figure S6.

Going back to eq 1, we can calculate the ratio of the radiative $A_{0\rightarrow1}$ for both complexes as

$$\frac{A^{t.w.}_{0\rightarrow1}}{A^{ref}_{0\rightarrow1}} = \frac{(n_{t.w.})^3 \cdot (\tilde{\nu}_{t.w.})^3}{(n_{ref})^3 \cdot (\tilde{\nu}_{ref})^3} = \frac{S^{t.w.}_{0\rightarrow1}}{S^{ref}_{0\rightarrow1}} \quad (2)$$

where t.w. and ref represent the quantities in this work [$Eu(btfa)_3(t\text{-}bpete)$] and for the reference sample($Eu(btfa)_3bipy$), respectively. $S_{0\rightarrow1}$ is the area under the $^5D_0 \rightarrow {}^7F_1$ transition. Rearranging eq 2, we obtain

https://dx.doi.org/10.1021/acs.langmuir.0c02862
Langmuir 2021, 37, 3248−3260

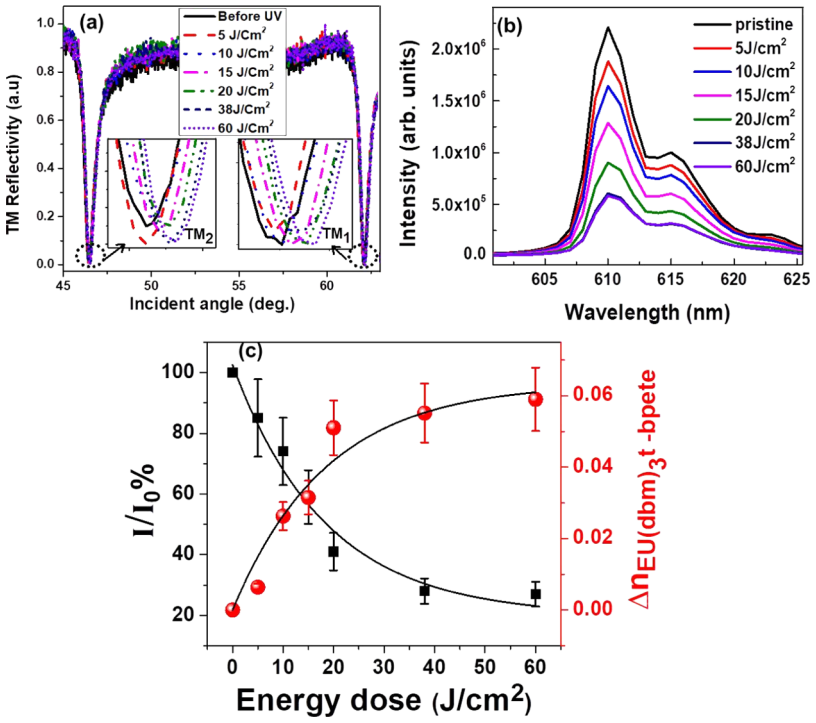

Figure 10. Experimental TM reflectivity curves of Au/SiO_2/Eu(btfa)$_3$(t-bpete) samples before and after UVA irradiation. (b) Emission spectra of encapsulated thin films of Eu(btfa)$_3$(t-bpete) as a function of different energy doses, excited at 360 nm. (c) Monitoring the refractive index (Δn) and PL intensity (I/I_0) variation of the Eu(btfa)$_3$(t-bpete) thin films under UVA irradiation in a nitrogen environment. The continuous lines represent the exponential fit of the experimental results. I_0 represents the intensity of the PL before UVA irradiation.

$$n_{\text{t.w.}} = n_{\text{ref}} \cdot \left(\frac{\tilde{\nu}_{\text{ref}}}{\tilde{\nu}_{\text{t.w.}}} \right) \cdot \sqrt[3]{\frac{S_{0\to1}^{\text{t.w.}}}{S_{0\to1}^{\text{ref}}}} \tag{3}$$

In the case of the Eu(btfa)$_3$bipy complex, when it is excited at 370 nm, the resulting emission spectrum is displayed in Figure 9a. The $^5D_0 \rightarrow {}^7F_1$ emission will be the reference for comparison with the same transition in the Eu(btfa)$_3$(t-bpete) film spectrum. However, since these two measurements were made under different conditions, to estimate the refractive index, it is necessary to normalize their $^5D_0 \rightarrow {}^7F_1$ intensities, as shown in Figure 9. The integrated areas (from 582.5 to 605.0 nm) are 7.99 and 10.74 (dimensionless because the curves of the $^5D_0 \rightarrow {}^7F_1$ transitions were normalized) for the reference and Eu(btfa)$_3$(t-bpete) samples, respectively. Table S3 shows all the necessary quantities and the refractive index estimation for the Eu(btfa)$_3$(t-bpete) film, giving a final value of 1.78.

Although the introduced spectroscopic model offers an indirect evaluation of the refractive index of the luminescent thin films, it confirms the high value obtained by the use of the DLWGs (n = 1.86), with a relative difference of only 5% between the results obtained by the two different experimental approaches.

4.2. UVA Sensor Based on Europium β-Diketonate Complex Thin Films on DLWGs. Recently, our group exploited the possibility to use the photo-instability of β-diketonate complexes for the development of UVA dosimeters.[23,50] In the case of Eu(btfa)$_3$(bipy) or Eu(dbm)$_3$phen thin films, the emission of organic materials is inversely proportional to the UV irradiation exposure, and SPR sensing also revealed a strict correlation between the refractive index increase and the quenching of the PL of Eu(dbm)$_3$phen thin films under UVA exposure.[23] This particular behavior is one of the reasons which also motivated us to investigate the Eu(btfa)$_3$(t-bpete) complex by DLWG spectroscopy, under external EM irradiation. In particular, the same two Au/SiO_2/Eu(btfa)$_3$(t-bpete) samples used for the thickness and dielectric constant characterization of the thin films were irradiated with controlled doses of UVA, and the shift of both the θ_{TM2} and θ_{TM1} resonance angles was monitored.

Figure 10a,b shows the dependence of the reflectivity spectra and of the PL ($^5D_0 \rightarrow {}^7F_2$ transition) intensity as a function of UVA energy doses (irradiation time), respectively. The refractive index of the Eu complex thin films measured in the previous section was used as the reference pre-irradiation value and the Δn variation in the refractive index with controlled UVA doses was measured experimentally. The experimental data points are represented as red closed circles in Figure 10c. The results of the parameters used for the fit on the experimental data by exponential functions are shown in Table S4.

As evident in Figure 10b, the exposure to UVA irradiation did not completely quench the PL of the organic material, and there is a residual PL intensity (I/I_0) of approximately 20% after the maximum dose of 60 J/cm^2. With UVA doses higher than 60 J/cm^2, there is almost no further variation in the value of the refractive index. Although the multimodal nature of the DLWGs allows the precise monitoring of changes in both the refractive index and thickness, the latter parameter was observed to be constant during UVA irradiation.

As observed in a previous work, where Alq_3 and Eu(dbm)$_3$phen were used as UVA sensing materials on monomodal SPR platforms,[23] the values of the energy constant (E_0) in the mathematical models used to fit both the PL decay and the refractive index enhancement of the Eu complex are the same within the experimental error. This interesting result

https://dx.doi.org/10.1021/acs.langmuir.0c02862
Langmuir 2021, 37, 3248−3260

means that both the refractive index and the PL intensity may be used successfully for the development of UVA dosimeters based on luminescent organic materials and that an intriguing correlation exists between different physical quantities.

5. CONCLUSIONS

We propose a protocol for the single measurement and simultaneous determination of the thickness (t_{film}) and dielectric constant (ε_{film}) of transparent thin films by DLWG spectroscopy. The protocol does not need the previous knowledge of t_{film} or ε_{film} like most of the monomodal SPR-based techniques reported in literature. The accuracy of DLWG thin-film characterization depends on the geometrical parameter of the WG, the thickness, and the dielectric constant of the transparent thin film under analysis, and the nature of the external environment (gas or liquid). Concerning the range, if an accuracy better than ∼15% is considered, the fabricated DLWGs can be successfully used for the characterization in nitrogen (air) of transparent thin films with thickness between 5 nm and the μm range, with values of the dielectric constant between 2 and 4. DLWG spectroscopy was applied for the special case of ∼20 nm thick luminescent thin films of Alq_3, $Eu(dbm)_3phen$, and $Eu(btfa)_3(t\text{-}bpete)$ encapsulated in a nitrogen environment, with an accuracy of about 4%. The high refractive index value measured for the $Eu(btfa)_3(t\text{-}bpete)$ complex is supported by a spectroscopic model based on Judd−Ofelt theory and the experimental PL intensity of the $^5D_0 \rightarrow {}^7F_1$ (Eu^{3+}) transition. In this case, PL and DLWG spectroscopy, which are used simultaneously for monitoring the refractive index changes induced by UV irradiation, are characterized by the same decay constant as a function of the energy dose, as previously reported for similar thin films. The presented multimodal DLWG approach may be applied to all the classes of transparent materials and is particularly attractive for UV dosimetry and applications related to light-induced physical−chemical transformations of thin films.

■ ASSOCIATED CONTENT

Supporting Information

The Supporting Information is available free of charge at https://pubs.acs.org/doi/10.1021/acs.langmuir.0c02862.

> TFT characterization of Alq_3, limits in the performance of the proposed DLWGs as thin-film characterization platforms, characterization of the Eu-based complex thin film by luminescence spectroscopy, and UVA response of europium β-diketonate complex thin films (PDF)

■ AUTHOR INFORMATION

Corresponding Authors

Quaid Zaman − *Department of Physics, Pontifícia Universidade Católica do Rio de Janeiro, 22451-900 Rio de Janeiro, Brazil*; Email: qzamanqau@gmail.com

Tommaso Del Rosso − *Department of Physics, Pontifícia Universidade Católica do Rio de Janeiro, 22451-900 Rio de Janeiro, Brazil*; orcid.org/0000-0002-0600-4139; Email: tommaso@puc-rio.br

Authors

Jefferson S. Costa − *Department of Electrical Engineering, Federal University of Pará, Belém 66075-110, Pará, Brazil*

Tahir − *Department of Physics, Pontifícia Universidade Católica do Rio de Janeiro, 22451-900 Rio de Janeiro, Brazil*; orcid.org/0000-0001-6565-5030

Arthur R. J. Barreto − *Department of Physics, Pontifícia Universidade Católica do Rio de Janeiro, 22451-900 Rio de Janeiro, Brazil*

Jefferson F. D. F. Araujo − *Department of Physics, Pontifícia Universidade Católica do Rio de Janeiro, 22451-900 Rio de Janeiro, Brazil*

Luís D. Carlos − *Phantom-g, CICECO-Aveiro Institute of Materials, Physics Department, University of Aveiro, 3810-193 Aveiro, Portugal*; orcid.org/0000-0003-4747-6535

Albano N. Carneiro Neto − *Phantom-g, CICECO-Aveiro Institute of Materials, Physics Department, University of Aveiro, 3810-193 Aveiro, Portugal*; orcid.org/0000-0003-2432-0992

Marco Cremona − *Department of Physics, Pontifícia Universidade Católica do Rio de Janeiro, 22451-900 Rio de Janeiro, Brazil*; orcid.org/0000-0003-1306-4639

Zubair Ahmed − *Department of Physics, Pontifícia Universidade Católica do Rio de Janeiro, 22451-900 Rio de Janeiro, Brazil*

André Felipe S. Cruz − *Department of Electrical Engineering, Federal University of Pará, Belém 66075-110, Pará, Brazil*

Nadson Welkson P. Souza − *Department of Electrical Engineering, Federal University of Pará, Belém 66075-110, Pará, Brazil*

Karlo Q. da Costa − *Department of Electrical Engineering, Federal University of Pará, Belém 66075-110, Pará, Brazil*

Victor Dmitriev − *Department of Electrical Engineering, Federal University of Pará, Belém 66075-110, Pará, Brazil*

Anna Laurenzana − *Department of Experimental and Clinical Biomedical Sciences, University of Florence, 50134 Florence, Italy*

Francesca Margheri − *Department of Experimental and Clinical Biomedical Sciences, University of Florence, 50134 Florence, Italy*

Complete contact information is available at: https://pubs.acs.org/10.1021/acs.langmuir.0c02862

Notes

The authors declare no competing financial interest.

■ ACKNOWLEDGMENTS

This study was financed in part by the Coordenação de Aperfeiçoamento de Pessoal de Nível Superior—Brasil (CAPES)—Finance Code 001. Funding from FAPERJ for processes E-26/010.002138/2019 and E-26/010.000980/2019 are acknowledged. Funding and scholarships from FAPESPA, CNPq, and INEO-INCT are also acknowledged.

■ REFERENCES

(1) Azzam, R. M. A.; Bashara, N. M. *Ellipsometry and Polarized Light*; Elsevier: Amsterdam, 1987.

(2) Fujiwara, H. *Spectroscopic Ellipsometry: Principles and Applications*; Wiley: Chichester, UK, 2007.

(3) Djurišić, A. B.; Kwong, C. Y.; Guo, W. L.; Lau, T. W.; Li, E. H.; Liu, Z. T.; Chan, W. K. Spectroscopic ellipsometry of the optical functions of tris (8-hydroxyquinoline) aluminum (Alq3). *Thin Solid Films* **2002**, *416*, 233−241.

(4) Himcinschi, C.; Meyer, N.; Hartmann, S.; Gersdorff, M.; Friedrich, M.; Johannes, H.-H.; Kowalsky, W.; Schwambera, M.; Strauch, G.; Heuken, M.; Zahn, D. R. T. Spectroscopic ellipsometric

characterization of organic films obtained via organic vapor phase deposition. *Appl. Phys. A* **2005**, *80*, 551−555.
(5) Pockrand, I.; Swalen, J. D.; Gordon, J. G.; Philpott, M. R. Surface plasmon spectroscopy of organic monolayer assemblies. *Surf. Sci.* **1978**, *74*, 237−244.
(6) Pockrand, I.; Swalen, J. D.; Santo, R.; Brillante, A.; Philpott, M. R. Optical properties of organic dye monolayers by surface plasmon spectroscopy. *J. Chem. Phys.* **1978**, *69*, 4001−4011.
(7) de Bruijn, H. E.; Altenburg, B. S. F.; Kooyman, R. P. H.; Greve, J. Determination of thickness and dielectric constant of thin transparent dielectric layers using Surface Plasmon Resonance. *Opt. Commun.* **1991**, *82*, 425−432.
(8) Del Rosso, T.; Sánchez, J. E. H.; Carvalho, R. D. S.; Pandoli, O.; Cremona, M. Accurate and simultaneous measurement of thickness and refractive index of thermally evaporated thin organic films by surface plasmon resonance spectroscopy. *Opt. Express* **2014**, *22*, 18914−18923.
(9) Raether, H. Surface Plasmons on Smooth and Rough Surfaces and on Gratings. *Springer Tracts in Modern Physics*; Springer-Verlag, 1988.
(10) Margheri, G.; Trigari, S.; Sottini, S.; D'Agostino, R.; Del Rosso, T.; Del Rosso, M. The binding of EGFR to GM1 (3) hosted in lipid raft-like biomembranes insighted by plasmonic resonance techniques. *J. Sens.* **2015**.
(11) Homola, J. Surface plasmon resonance sensors for detection of chemical and biological species. *Chem. Rev.* **2008**, *108*, 462−493.
(12) Sadowski, J. W.; Korhonen, I. K.; Peltonen, J. P. Characterization of thin films and their structures in surface plasmon resonance measurements. *Opt. Eng.* **1995**, *34*, 2581−2587.
(13) Peterlinz, K. A.; Georgiadis, R. Two-color approach for determination of thickness and dielectric constant of thin films using surface plasmon resonance spectroscopy. *Opt. Commun.* **1996**, *130*, 260−266.
(14) Costa, J.; Zaman, Q.; Q. da Costa, K.; Dmitriev, V.; Pandoli, O.; Fontes, G.; Del Rosso, T. Limits of the effective medium theory in particle amplified surface plasmon resonance spectroscopy biosensors. *Sensors* **2019**, *19*, 584.
(15) Salamon, Z.; Macleod, H. A.; Tollin, G. Coupled plasmon-waveguide resonators: a new spectroscopic tool for probing proteolipid film structure and properties. *Biophys. J.* **1997**, *73*, 2791−2797.
(16) Knoll, W. Interfaces and Thin Films as seen by bound Electromagnetic Waves. *Annu. Rev. Phys. Chem.* **1998**, *49*, 569−638.
(17) Zaman, Q.; Souza, J.; Pandoli, O.; Costa, K. Q.; Dmitriev, V.; Fulvio, D.; Cremona, M.; Aucelio, R. Q.; Fontes, G.; Del Rosso, T. Two-color surface plasmon resonance nanosizer for gold nanoparticles. *Opt. Express* **2019**, *27*, 3200−3216.
(18) Chen, Q. Stability of an ultrathin plasma polymerized film in aqueous solution: In situ detection by surface plasmon resonance. *J. Phys. Chem. B* **2006**, *110*, 9231−9235.
(19) Akhavan, B.; Menges, B.; Förch, R. Inhomogeneous growth of micrometer thick plasma polymerized films. *Langmuir* **2016**, *32*, 4792−4799.
(20) Kido, J.; Okamoto, Y. Organo lanthanide metal complexes for electroluminescent materials. *Chem. Rev.* **2002**, *102*, 2357−2368.
(21) Barrientos, H.; Arias, E.; Moggio, I.; Romero, J.; Rodríguez, O.; Giorgetti, E.; Rosso, T. D. Dodecanoxy-phenylethynylene oligomers for light emitting diodes. *Synth. Met.* **2004**, *147*, 267−270.
(22) Koen, B. Lanthanide-based luminescent hybrid materials. *Chem. Rev.* **2009**, *109*, 4283−4374.
(23) Del Rosso, T.; Zaman, Q.; Cremona, M.; Pandoli, O.; Barreto, A. R. J. SPR sensors for monitoring the degradation processes of Eu(dbm)3(phen) and Alq3 thin films under atmospheric and UVA exposure. *Appl. Surf. Sci.* **2018**, *442*, 759−766.
(24) Lee, K. S.; Lee, M.; Byun, K. M.; Lee, I. S. Surface plasmon resonance biosensing based on target-responsive mobility switch of magnetic nanoparticles under magnetic fields. *J. Mater. Chem.* **2011**, *21*, 5156−5162.
(25) Giorgetti, E.; Muniz-Miranda, M.; Giusti, A.; DelRosso, T.; Dellepiane, G.; Margheri, G.; Sottini, S.; Alloisio, M.; Cuniberti, C. Spectroscopic investigation on the in situ polymerization of self assembled monolayers of carbazolyldiacetylene CDS9 on silver-coated glass. *Thin Solid Films* **2006**, *495*, 36−39.
(26) Tanchak, O. M.; Barrett, C. J. Light-induced reversible volume changes in thin films of azo polymers: the photomechanical effect. *Macromolecules* **2005**, *38*, 10566−10570.
(27) Lima, P. P.; Nolasco, M. M.; Paz, F. A. A.; Ferreira, R. A. S.; Longo, R. L.; Malta, O. L.; Carlos, L. D. Photo-Click Chemistry to Design Highly Efficient Lanthanide β-Diketonate Complexes Stable under UV Irradiation. *Chem. Mater.* **2013**, *25*, 586−598.
(28) Del Rosso, T.; Zaman, Q.; Romani, E. C.; Pandoli, O.; Aucelio, R. Q.; Melo de Lima, L.; Cremona, M.; Dmitriev, V.; Queiroz da Costa, K.; Lazaro Freire, F.; Maia da Costa, M. E. H. Enhanced stability of plasmonic metal thin films by CVD grown graphene transfer. *Thin Solid Films* **2017**, *644*, 65−70.
(29) Chen, X.; Jiang, K. Effect of aging on optical properties of bimetallic sensor chips. *Opt. Express* **2010**, *18*, 1105−1112.
(30) Piwonski, I.; Grobelny, J.; Cichomski, M.; Celichowski, G.; Rogowski, J. Investigation of 3- mercaptopropyltrimethoxysilane self-assembled monolayers on Au (111) surface. *Appl. Surf. Sci.* **2005**, *242*, 147−153.
(31) Worm, J. *Winspall 2.20 Software*, 2001, http://www.mpip-mainz.mpg.de/johanns/winspall2.ZIP.
(32) Walpita, L. M. Solutions for planar optical waveguide equations by selecting zero elements in a characteristic matrix. *J. Opt. Soc. Am. A* **1985**, *2*, 595−602.
(33) Wang, D.; Zheng, C.; Fan, L.; Zheng, J.; Wei, X. Preparation and fluorescent properties of europium (III) complexes with β-diketone ligand and 2, 2-dipyridine or 1, 10-phenanthroline. *Synth. Met.* **2012**, *162*, 2063−2068.
(34) Teotonio, E. E. S.; Brito, H. F.; de Sá, G. F.; Felinto, M. C. F. C.; Santos, R. H. A.; Fuquen, R. M.; Costa, I. F.; Kennedy, A. R.; Gilmore, D.; Faustino, W. M. Structure and luminescent investigation of the Ln (III)−β-diketonate complexes containing tertiary amides. *Polyhedron* **2012**, *38*, 58−67.
(35) Malta, O. L.; Brito, H. F.; Menezes, J. F. S.; Silva, F. R. G. e., Jr.; Alves, S., Jr.; Farias, F. S.; de Andrade, A. V. M. Spectroscopic properties of a new light-converting device Eu-(thenoyltrifluoroacetonate)3 2(dibenzyl sulfoxide). A theoretical analysis based on structural data obtained from a sparkle model. *J. Lumin.* **1997**, *75*, 255−268.
(36) Homola, J.; Yee, S. S.; Gauglitz, G. Surface plasmon resonance sensors: review. *Sens. Actuators, B* **1999**, *54*, 3−15.
(37) Liedberg, B.; Nylander, C.; Lundström, I. Biosensing with surface plasmon resonance—how it all started. *Biosens. Bioelectron.* **1995**, *10*, i−ix.
(38) Lee, W.; Kim, D. Field-matter integral overlap to estimate the sensitivity of surface plasmon resonance biosensors. *J. Opt. Soc. Am. A* **2012**, *29*, 1367−1376.
(39) Shalabney, A.; Abdulhalim, I. Electromagnetic fields distribution in multilayer thin film structures and the origin of sensitivity enhancement in surface plasmon resonance sensors. *J. Opt. Soc. Am. A* **2010**, *159*, 24−32.
(40) Yariv, A. Coupled-mode theory for guided-wave optics. *IEEE J. Quantum Electron.* **1973**, *9*, 919−933.
(41) Elhadj, S.; Singh, G.; Saraf, R. F. Optical properties of an immobilized DNA monolayer from 255 to 700 nm. *Langmuir* **2004**, *20*, 5539−5543.
(42) Tompkins, H. G. I.; Eugene, A. *A Handbook of Ellipsometry*; William Andrew Publishing: New York, 2005.
(43) Hall, A. C. On the use of ellipsometry for adsorption measurements below monolayer coverage. *J. Phys. Chem.* **1966**, *70*, 1702−1704.
(44) Johs, B.; Herzinger, C. M. Quantifying the accuracy of ellipsometer systems. *Phys. Status Solidi C* **2008**, *5*, 1031−1035.
(45) https://www.horiba.com/en_en/products/detail/action/show/Product/smart-se-1105/, accessed December 2020.

https://dx.doi.org/10.1021/acs.langmuir.0c02862
Langmuir 2021, 37, 3248−3260

(46) Carneiro Neto, A. N.; Teotonio, E. E. S.; de Sa, G. F.; Brito, H. F.; Legendziewicz, J.; Carlos, L. D.; Felinto, M. C. F. C.; Gawryszewska, P.; Moura, R. T., Jr.; Longo, R. L.; Faustino, W. M.; Malta, O. L. Modeling Intramolecular Energy Transfer in Lanthanide Chelates: A Critical Review and Recent Advances. *Handbook on the Physics and Chemistry of Rare Earths*; Elsevier, 2019; Vol. *56*, Chapter 310, pp 55−162.
(47) Ofelt, G. S. Intensities of crystal spectra of rare-earth ions. *J. Chem. Phys.* **1962**, *37*, 511−520.
(48) Felinto Brito, H.; Manoel Loureiro Malta, O.; Claudia França Cunha Felinto, M.; Epaminondas de Sousa Teotonio, E. *Luminescence Phenomena Involving Metal Enolates*; PATAI'S Chemistry of Functional Groups, 2009.
(49) de Sá, G. F.; Alves, S., Jr.; da Silva, B. J. P.; da Silva, E. F., Jr. A novel fluorinated Eu(III) β-diketone complex as thin film for optical device applications. *Opt. Mater.* **1998**, *11*, 23−28.
(50) Quirino, W.; Reyes, R.; Legnani, C.; Nóbrega, P. C.; Santa-Cruz, P. A.; Cremona, M. Eu-β-diketonate complex OLED as UV portable dosimeter. *Synth. Met.* **2011**, *161*, 964−968.

https://dx.doi.org/10.1021/acs.langmuir.0c02862
Langmuir 2021, 37, 3248−3260